Pergamon

Int. J. Solids Structures Vol. 33, No. 27, pp. 3983–4005, 1996

0020-7683/96 $15.00 + .00

0020-7683(95)00221-9

SEMI-ANALYTICAL SOLUTION OF 2-D ELASTICITY PROBLEMS BY THE STRIP DISTRIBUTED TRANSFER FUNCTION METHOD

B. YANG and J. ZHOU
Department of Mechanical Engineering, University of Southern California, Los Angeles, CA 90089-1453, U.S.A.

(*Received* 23 *January* 1995; *in revised form* 8 *September* 1995)

Abstract—A new technique, called the strip distributed transfer function method, is developed for static and dynamic analysis of two-dimensional elastic bodies that are composed of multiple rectangular subregions. The method is capable of modeling elastic regions of complex geometry and arbitrary boundary conditions, delivers highly accurate semi-analytical solutions and saves tremendous computer storage. In the analysis, a complex elastic region is first divided into a number of subregions; each subregion is then divided into finite strips. Through introduction of strip distributed transfer functions, the response of every subregion is presented in a semi-exact and closed form; the whole region is systematically assembled from the subregions, leading to a dynamic equilibrium equation. Solution of the equilibrium equation yields the semi-exact displacements and stresses of the elastic body. The proposed method is illustrated on a square region and an L-shaped region, and compared with the finite element method. Copyright © 1996 Elsevier Science Ltd

1. INTRODUCTION

A semi-analytical technique is presented for static and dynamic analysis of two-dimensional, linear elasticity problems in regions that are composed of multiple rectangular subregions. The technique, called the strip distributed transfer function method (SDTFM), is capable of treating complex geometry and general boundary conditions, provides highly accurate solutions, and greatly reduces data storage in computation.

Elasticity problems are often studied by numerical methods because exact solutions are only available for very few simple examples. As a powerful numerical tool, the finite element method (FEM) is widely used in elasticity problems (Zienkwicz and Tailor, 1989). One obvious advantage of FEM is its flexibility in modeling elastic bodies of complicated geometry, different material properties, and arbitrary boundary conditions. However, this flexibility of FEM is at the cost of large computer storage and CPU time, and sometimes is devalued by the need for real-time computations, as in the case of active control of elastic systems. Additionally, FEM may lose accuracy in predicting high-gradient stress distributions, and high-frequency dynamic response of elastic bodies.

The finite strip method is another numerical method that has been applied to elasticity problems (Cheung, 1976). In this method, an elastic region is divided into a number of strips; the strip displacements in the strip lateral and longitudinal coordinates are approximated by polynomials, and series of continuous functions, respectively. It has been shown that the finite strip method requires much less computer memory. Nonetheless, the finite strip method is limited to certain regular shapes, and requires increased computer memory to deal with concentrated loads, pointwise constraints, and abrupt changes in geometric and material properties.

The are other numerical methods, usually of Ritz or Galerkin type. These methods present solutions by series of continuous functions that satisfy prescribed boundary conditions. The selection of these admissible comparison functions is done on a problem-by-problem basis, and is difficult even for some regions of simple geometry. Also, high accuracy of series solutions relies on a large number of functions in the series. These features prevent the application of series solution methods from extending to general elastic regions.

The current investigation is motivated by the desire to have a technique which combines the flexibility of FEM in treating complex geometry, and the closed form and high accuracy of analytical solutions. The flexibility of FEM lies in that the element displacement functions are interpolated in nodal parameters, which are the displacements at the selected points on the element boundaries. The number of terms in the element interpolation functions is identical to that of nodal parameters. In this way, a complex shape can be conveniently assembled from those finite elements via imposing continuity and equilibrium conditions on the element functions. Extending the assembly concept of FEM, if for some basic elastic regions, one can find closed-form, analytical or semi-analytical solutions that are expressible by "nodal parameters", then using these regions as "super elements", one can construct highly accurate and memory-saving solutions for regions of complex shapes.

The SDTFM proposed in this work is based on the above idea. This method is an extension of the distributed transfer function method for one-dimensional distributed parameter systems (Yang, 1989, 1992, and 1994; Yang and Tan, 1992). In the analysis, a rectangular subregion is divided into finite strips. The strip displacements are interpolated in the nodal line displacements, which are the unknown displacement functions defined on several longitudinal lines of the strips. Unlike the finite strip method and the existing series solution methods, SDTFM does not utilize series expansion of particular admissible/comparison functions to determine the nodal line displacements. Instead, it expresses the nodal line displacements by the so-called strip distributed transfer functions, which are defined in an exact and closed state-space form. The transfer function formulation allows explicit representation of the response of the subregion by the displacements at the selected boundary points of the subregion. As such, assembly of subregions can be done similarly as in FEM, which eventually leads to a global dynamic equilibrium equation. Solution of the global equation gives accurate prediction of static and dynamic response (displacements, strains and stresses) for many complex 2-D elastic regions.

The remainder of this paper is arranged as follows. Rectangular elastic regions are analyzed in Section 2, where the strips and nodal line displacements are defined, and strip distributed transfer functions are introduced. Assembly of multiple rectangular subregions is studied in Section 3. Three models of strip displacement interpolation are derived in Section 4. The proposed method is illustrated on a square region and an L-shaped region in Section 5, where the numerical results obtained by SDTFM and FEM are compared. The advantages of the proposed method are further discussed in Section 6.

2. ANALYSIS OF RECTANGULAR ELASTIC REGIONS

The 2-D elasticity problem in a region Ω is described by the Hamilton's principal

$$\int_0^t \left\{ \frac{1}{2}\delta \int_\Omega (\{\varepsilon\}^T[\mathbf{A}]\{\varepsilon\} - \rho h\{\dot{\mathbf{u}}\}^T\{\dot{\mathbf{u}}\})\,d\Omega - \int_\Omega \{\delta\mathbf{u}\}^T\{\mathbf{f}\}\,d\Omega - \int_{\Gamma_\sigma} \{\delta\mathbf{u}\}^T\{\bar{\mathbf{T}}_\sigma\}\,d\Gamma \right\} dt = 0 \tag{1}$$

where $\{\mathbf{u}\}$ and $\{\varepsilon\}$ are the displacement and strain vectors of the form

$$\{\mathbf{u}\} = \begin{Bmatrix} u \\ v \end{Bmatrix}, \quad \{\varepsilon\} = \left\{ \frac{\partial u}{\partial x} \quad \frac{\partial v}{\partial y} \quad \frac{\partial u}{\partial y} + \frac{\partial v}{\partial x} \right\}^T \tag{2}$$

$\{\dot{\mathbf{u}}\} = \partial\{\mathbf{u}\}/\partial t$, $\{\delta\mathbf{u}\}$ is the variation of $\{\mathbf{u}\}$, $\{\mathbf{f}\}$ is the vector of body forces, ρ is mass per unit volume, h is the thickness of the elastic region, $\{\bar{\mathbf{T}}_\sigma\}$ are the external tractions vector, and Γ_σ is the part of the boundary of Ω on which external tractions are prescribed. For anisotropic elastic material, the constitutive matrix is given by

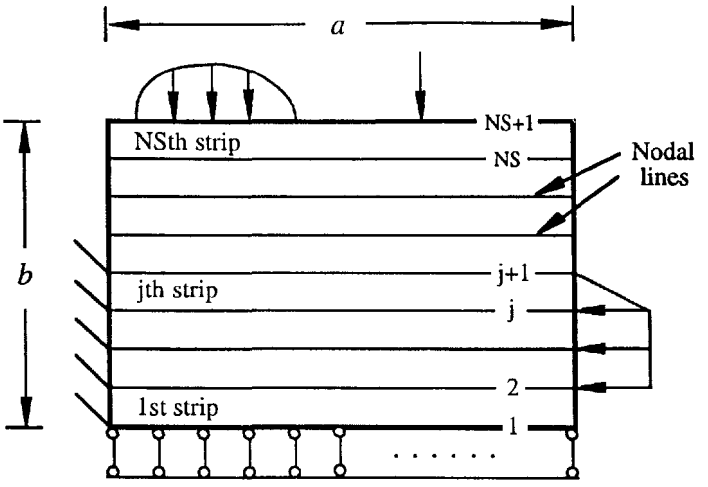

Fig. 1. A rectangular region divided into strips.

$$[\mathbf{A}] = h \begin{bmatrix} C_{11} & C_{12} & C_{16} \\ C_{12} & C_{22} & C_{26} \\ C_{16} & C_{26} & C_{66} \end{bmatrix} \tag{3}$$

where C_{ij} are the elastic constants.

In this section, rectangular regions are analyzed. Assembly of rectangular subregions will be addressed in Section 3. In analysis of a rectangular region, the proposed method (SDTFM) takes three steps: (i) it divides the region into a number of rectangular strips, and interpolates the displacements of each strip in nodal line displacement parameters; (ii) it assembles the region from the strips, yielding a matrix dynamic equation governing the nodal line displacements; and (iii) it obtains exact and closed-form solution for the nodal line displacements in terms of strip distributed transfer functions, leading to semi-analytical solutions for various static and dynamic problems of the 2-D region. These steps are detailed in the following three subsections.

2.1. *Definition of strips and interpolation of strip displacements*

In Fig. 1 a rectangular region of length a and width b is divided into NS rectangular strips by NS+1 lines, which are called nodal lines. The two ends of each nodal line are called nodes. The jth strip is defined by the jth and $(j+1)$th nodal lines and four nodes; see Fig. 2(a), where b_j is the strip width, and oxy is a local coordinate system with the origin located at the middle of the strip bottom. In addition, internal nodal lines may be introduced within a strip; see Fig. 2(b).

Along the jth nodal line, denote the displacement functions u and v by u_j and v_j, and the derivatives $\partial u/\partial y$ and $\partial v/\partial y$ by u_{yj} and v_{yj}. These parameters, which are functions of the

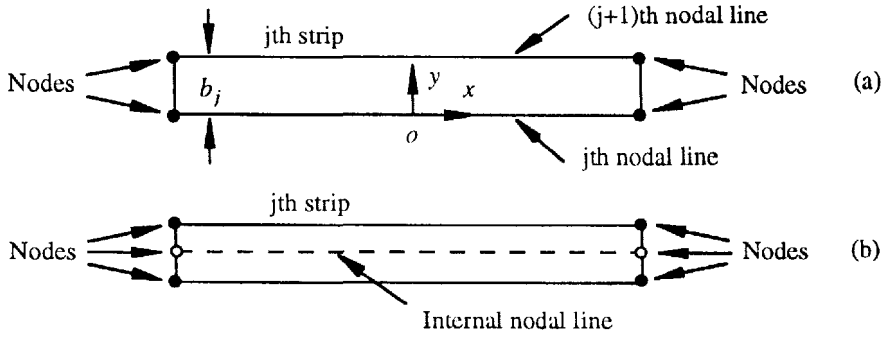

Fig. 2. The jth strip without or with an internal nodal line.

spatial coordinate x and time t, are called nodal line displacements. Let the vector $\psi_j(x,t)$ consist of some or all of the above-defined displacement parameters of the jth nodal line. For example, $\psi_j(x,t)$ can be $\{u_j(x,t)\ v_j(x,t)\}^T$ or $\{u_j(x,t)\ v_j(x,t)\ u_{yj}(x,t)\ v_{yj}(x,t)\}^T$; see Section 4. Similarly, a vector $\lambda_j(x,t)$ of the displacement parameters on some internal nodal lines of the strip can be defined.

Define the nodal line displacement vector of the jth strip by

$$\{\mathbf{U}_j(x,t)\} = \{\psi_j^T(x,t) \quad \lambda_j^T(x,t) \quad \psi_{j+1}^T(x,t)\}^T \tag{4}$$

The displacements of the jth strip are interpolated in the nodal line displacements by

$$\{\mathbf{u}(x,t)\} = \begin{Bmatrix} u(x,t) \\ v(x,t) \end{Bmatrix} = [\mathbf{N}(y)]\{\mathbf{U}_j(x,t)\} = \begin{bmatrix} [\mathbf{N}_u(y)] \\ [\mathbf{N}_v(y)] \end{bmatrix} \{\mathbf{U}_j(x,t)\} \tag{5}$$

where $[\mathbf{N}(y)]$ is the matrix of shape functions. To guarantee convergence, the shape functions must be able to describe a state of constant strain in the y-direction, and to assure C_0-continuity of the displacements across the mutual boundaries (nodal lines) of the strips. Examples of shape functions are given in Section 4.

2.2. *Dynamic equation of nodal line displacements*

Substituting (5) into (2) gives

$$\{\varepsilon\} = \left([\mathbf{B}_{u,0}] + [\mathbf{B}_{u,1}] \frac{\partial}{\partial x} \right) \{\mathbf{U}_j\} \tag{6}$$

where

$$[\mathbf{B}_{u,0}] = \frac{\mathrm{d}}{\mathrm{d}y} \begin{bmatrix} [0] \\ [\mathbf{N}_v] \\ [\mathbf{N}_u] \end{bmatrix}, \quad [\mathbf{B}_{u,1}] = \begin{bmatrix} [\mathbf{N}_u] \\ [0] \\ [\mathbf{N}_v] \end{bmatrix} \tag{7}$$

By (5) and (6), the Hamilton's principal (1) becomes

$$\sum_{j=1}^{NS} \int_0^t \left\{ \frac{1}{2}\delta \int_{-0.5a}^{0.5a} (\{\mathbf{U}_j'\}^T[\mathbf{k}_{11}^j]\{\mathbf{U}_j'\} + 2\{\mathbf{U}_j\}^T[\mathbf{k}_{01}^j]\{\mathbf{U}_j'\} + \{\mathbf{U}_j\}^T[\mathbf{k}_{00}^j]\{\mathbf{U}_j\} \right.$$
$$\left. - \{\dot{\mathbf{U}}_j\}^T[\mathbf{m}^j]\{\dot{\mathbf{U}}_j\})\,\mathrm{d}x - \int_{-0.5a}^{0.5a} \{\delta\mathbf{U}_j\}^T\{\mathbf{q}_u^j\}\,\mathrm{d}x + \{\delta\mathbf{U}_j\}^T\{\bar{\mathbf{S}}_j\}|_{x=\pm 0.5a} \right\} \mathrm{d}t \tag{8}$$

where $\{\mathbf{U}_j'\} = \partial\{\mathbf{U}_j\}/\partial x$, $\{\dot{\mathbf{U}}_j\} = \partial\{\mathbf{U}_j\}/\partial t$, and

$$[\mathbf{k}_{00}^j] = \int_0^{b_j} [\mathbf{B}_{u,0}]^T[\mathbf{A}][\mathbf{B}_{u,0}]\,\mathrm{d}y, \quad [\mathbf{k}_{01}^j] = \int_0^{b_j} [\mathbf{B}_{u,0}]^T[\mathbf{A}][\mathbf{B}_{u,1}]\,\mathrm{d}y$$

$$[\mathbf{k}_{11}^j] = \int_0^{b_j} [\mathbf{B}_{u,1}]^T[\mathbf{A}][\mathbf{B}_{u,1}]\,\mathrm{d}y, \quad [\mathbf{m}^j] = \int_0^{b_j} \rho h[\mathbf{N}]^T[\mathbf{N}]\,\mathrm{d}y$$

$$\{\mathbf{q}_u^j\} = \int_0^{b_j} [\mathbf{N}]^T\{\mathbf{f}\}\,\mathrm{d}y, \quad \{\bar{\mathbf{S}}_j\} = \int_0^{b_j} [\mathbf{N}]^T\{\bar{\mathbf{T}}_\sigma\}\,\mathrm{d}y.$$

Here $[\mathbf{k}_{00}^j]$, $[\mathbf{k}_{01}^j]$ and $[\mathbf{k}_{11}^j]$ are called the strip stiffness matrices, $[\mathbf{m}^j]$ the strip mass matrix, $\{\mathbf{q}_u^j\}$ the strip body force vector, and $\{\bar{\mathbf{S}}_j\}$ the generalized nodal force vector.

Now introduce the global nodal line displacement vector

$$\{\Phi_u\} = \{\psi_1^T \quad \lambda_1^T \quad \psi_2^T \ldots \lambda_{NS}^T \quad \psi_{NS+1}^T\}^T \tag{9}$$

where $\{\psi_j\}$ and $\{\lambda_j\}$ have been given in (4). In terms of $\{\Phi_u\}$, (8) reduces to

$$\int_0^t \left\{ \frac{1}{2}\delta \int_{-0.5a}^{0.5a} (\{\Phi_u'\}^T[\mathbf{K}_{11}]\{\Phi_u'\} + 2\{\Phi_u\}^T[\mathbf{K}_{01}]\{\Phi_u'\} + \{\Phi_u\}^T[\mathbf{K}_{00}]\{\Phi_u\} - \{\dot{\Phi}_u\}^T[\mathbf{M}]\{\dot{\Phi}_u\})\,dx - \int_{-0.5a}^{0.5a} \{\delta\Phi_u\}^T\{\mathbf{Q}_u\}\,dx - \{\delta\Phi_u\}^T\{\bar{\mathbf{S}}\}|_{x=\pm 0.5a} \right\} dt \tag{10}$$

where $[\mathbf{K}_{00}]$, $[\mathbf{K}_{01}]$ and $[\mathbf{K}_{11}]$ are the global stiffness matrices, $[\mathbf{M}]$ the global mass matrix, $\{\mathbf{Q}_u\}$ the global body force vector, and $\{\bar{\mathbf{S}}\}$ the global generalized nodal force vector. These matrixes and vectors are assembled from those in (8) the same way as in the finite element analysis; i.e.,

$$\{\Phi_u'\}^T[\mathbf{K}_{11}]\{\Phi_u'\} = \sum_{j=1}^{NS} \{\mathbf{U}_j'\}^T[\mathbf{k}_{11}^j]\{\mathbf{U}_j'\},\ \{\delta\Phi_u\}^T\{\mathbf{Q}_u\} = \sum_{j=1}^{NS} \{\delta\mathbf{U}_j\}^T\{\mathbf{q}_u^j\}, \text{etc.}$$

Variation of $\{\Phi_u\}$ in (10) and integral by part lead to

$$\{\delta\Phi_u\}^T\left(\left([\mathbf{M}]\frac{\partial^2}{\partial t^2} - [\mathbf{K}^{(2)}]\frac{\partial^2}{\partial x^2} + \sum_{i=0}^{1}[\mathbf{K}^{(i)}]\frac{\partial^i}{\partial x^i}\right)\{\Phi_u\} - \{\mathbf{Q}_u\}\right) = 0, \quad x \in (-0.5a, 0.5a) \tag{11a}$$

$$\{\delta\Phi_u\}^T(\{\bar{\mathbf{S}}\} - \mathrm{sgn}(x)([\mathbf{K}_{01}]^T\{\Phi\} + [\mathbf{K}_{11}]\{\Phi_u'\}))|_{x=\pm 0.5a} = 0 \tag{11b}$$

where $[\mathbf{K}^{(2)}] = [\mathbf{K}_{11}]$, $[\mathbf{K}^{(1)}] = [\mathbf{K}_{01}] - [\mathbf{K}_{01}]^T$, $[\mathbf{K}^{(0)}] = [\mathbf{K}_{00}]$, and $\mathrm{sgn}(x) = 1$ (-1) for $x > 0$ (>0).

When $\{\delta\Phi_u\}$ is arbitrary, the dynamic equation by (11a) is:

$$\left([\mathbf{M}]\frac{\partial^2}{\partial t^2} - [\mathbf{K}^{(2)}]\frac{\partial^2}{\partial x^2} + \sum_{i=0}^{1}[\mathbf{K}^{(i)}]\frac{\partial^i}{\partial x^i}\right)\{\Phi_u\} = \{\mathbf{Q}_u\}. \tag{12}$$

However, $\{\delta\Phi_u\}$ is not arbitrary if a nodal line displacement is known or specified. For instance, if the jth nodal line is clamped, i.e., $u_j(x, t) = v_j(x, t) = 0$ for $x \in (-0.5a, 0.5a)$, δu_j and δv_j can only be zero. In this case, the dynamic equation is derived by eliminating those known nodal line displacements from $\{\Phi_u\}$.

Let $\{\Phi_u\}$ have N unknown nodal line displacements, denoted by the vector $\{\phi\}$, and $\bar{N}$ known nodal line displacements, denoted by the vector $\{\bar{\phi}\}$. Rearranging the elements of $\{\phi\}$ and $\{\bar{\phi}\}$ in $\{\Phi_u\}$, one obtains

$$\{\Phi_u\} = [\mathbf{T}]\begin{Bmatrix}\phi\\ \bar{\phi}\end{Bmatrix} = [\mathbf{T}_1]\{\phi\} + [\mathbf{T}_2]\{\bar{\phi}\} \tag{13}$$

where $[\mathbf{T}] = [\mathbf{T}_1\ \mathbf{T}_2]$ is a row transformation matrix with the sub-matrices $[\mathbf{T}_1]$ and $[\mathbf{T}_2]$ of proper dimensions. For example, if $\{\Phi_u\} = \{\phi_1 \quad \bar{\phi}_2 \quad \phi_2 \quad \bar{\phi}_1\}^T$, then

$$\{\Phi\}_u = \begin{bmatrix} 1 & 0 & 0 & 0 \\ 0 & 0 & 0 & 1 \\ 0 & 1 & 0 & 0 \\ 0 & 0 & 1 & 0 \end{bmatrix} \begin{Bmatrix} \phi_1 \\ \phi_2 \\ \bar{\phi}_1 \\ \bar{\phi}_2 \end{Bmatrix} = \begin{bmatrix} 1 & 0 \\ 0 & 0 \\ 0 & 1 \\ 0 & 0 \end{bmatrix} \begin{Bmatrix} \phi_1 \\ \phi_2 \end{Bmatrix} + \begin{bmatrix} 0 & 0 \\ 0 & 1 \\ 0 & 0 \\ 1 & 0 \end{bmatrix} \begin{Bmatrix} \bar{\phi}_1 \\ \bar{\phi}_2 \end{Bmatrix}.$$

Plugging (13) into (11), letting $\{\delta\bar{\phi}\} = 0$, and conducting arbitrary variation of $\{\phi\}$, one obtains the dynamic equation governing the unknown nodal line displacements

$$\left([\bar{\mathbf{M}}]\frac{\partial^2}{\partial t^2} - [\bar{\mathbf{K}}^{(2)}]\frac{\partial^2}{\partial x^2} + \sum_{i=0}^{1}[\bar{\mathbf{K}}^{(i)}]\frac{\partial^i}{\partial x^i}\right)\{\phi\} = \{\mathbf{Q}_\phi\} \tag{14}$$

and the boundary conditions

$$\{\delta\phi\}^{\mathrm{T}}([\Pi_\phi]\{\phi\} - \{\mathbf{S}_\phi\})|_{x=\pm 0.5a} = 0 \tag{15}$$

where

$$[\bar{\mathbf{M}}] = [\mathbf{T}_1]^{\mathrm{T}}[\mathbf{M}][\mathbf{T}_1]; \quad [\bar{\mathbf{K}}^{(i)}] = [\mathbf{T}_1]^{\mathrm{T}}[\mathbf{K}^{(i)}][\mathbf{T}_1], \quad i = 0, 1, 2$$

$$[\mathbf{Q}_\phi\} = [\mathbf{T}_1]^{\mathrm{T}}\{\mathbf{Q}_u\} - [\mathbf{T}_1]^{\mathrm{T}}\left([\mathbf{M}]\frac{\partial^2}{\partial t^2} - [\mathbf{K}^{(2)}]\frac{\partial^2}{\partial x^2} + \sum_{i=0}^{1}[\mathbf{K}^{(i)}]\frac{\partial^i}{\partial x^i}\right)[\mathbf{T}_2]\{\bar{\phi}\}$$

$$[\Pi_\phi] = [\mathbf{T}_1]^{\mathrm{T}}\left([\mathbf{K}_{01}]^{\mathrm{T}} + [\mathbf{K}_{11}]\frac{\partial}{\partial x}\right)[\mathbf{T}_1]$$

$$\{\mathbf{S}_\phi\}|_{x=\pm 0.5a} = \left\{[\mathbf{T}_1]^{\mathrm{T}}\{\bar{\mathbf{S}}\} - \mathrm{sgn}(x)[\mathbf{T}_1]^{\mathrm{T}}\left([\mathbf{K}_{01}]^{\mathrm{T}} + [\mathbf{K}_{11}]\frac{\partial}{\partial x}\right)[\mathbf{T}_2]\{\bar{\phi}\}\right\}\Big|_{x=\pm 0.5a}$$

2.3. *Solution by strip distributed transfer functions*

The dynamic eqn (14) is solved in the Laplace transform domain by a state-space technique. Laplace transform of (14) with respect to time gives

$$\frac{\partial^2}{\partial x^2}\{\hat{\phi}(x,s)\} = [\mathbf{A}_1]\frac{\partial}{\partial x}\{\hat{\phi}(x,s)\} + [\mathbf{A}_2(s)]\{\hat{\phi}(x,s)\} + \{\mathbf{Q}_{el}(x,s)\} \tag{16}$$

where the carat $\hat{}$ denotes Laplace transformation, s is the complex Laplace transform parameter, and

$$[\mathbf{A}_1] = [\bar{\mathbf{K}}^{(2)}]^{-1}[\bar{\mathbf{K}}^{(1)}], \quad [\mathbf{A}_2(s)] = [\bar{\mathbf{K}}^{(2)}]^{-1}([\bar{\mathbf{K}}^{(0)}] + s^2[\bar{\mathbf{M}}])$$

$$\{\mathbf{Q}_{el}(x,s)\} = -[\bar{\mathbf{K}}^{(2)}]^{-1}(\{\hat{\mathbf{Q}}_\phi(x,s)\} + [\bar{\mathbf{M}}](s\{\phi\} + \{\dot{\phi}\})|_{t=0}).$$

The boundary conditions for (16) are derived from (15). Let $\{\hat{\mathbf{S}}_\phi\}$ be the Laplace transform of $\{\mathbf{S}_\phi\}$. Write

$$\{\hat{\phi}(x,s)\} = \begin{Bmatrix} \hat{\phi}_1(x,s) \\ \vdots \\ \hat{\phi}_N(x,s) \end{Bmatrix}, \quad \{\hat{\mathbf{S}}_\phi\}|_{x=\pm 0.5a} = \begin{Bmatrix} \tau_1^{\pm}(s) \\ \vdots \\ \tau_N^{\pm}(s) \end{Bmatrix}, \quad [\Pi_\phi] = \begin{bmatrix} \pi_1 \\ \vdots \\ \pi_N \end{bmatrix}. \tag{17}$$

Here N is the number of unknown nodal line displacements, $\tau_j^+(s)$ and $\tau_j^-(s)$ represent the specified forces at the right and left nodes ($x = \pm 0.5a$) of the nodal line on which the jth

unknown nodal line displacement is defined, respectively, and π_k is the kth row of the matrix operator $[\Pi_\phi]$. By (15), there are two pairs of boundary conditions for each nodal line displacement; i.e.,

$$\text{at } x = -0.5a \quad \hat{\phi}_j = \alpha_j^- (s) \quad \text{or} \quad \pi_j \hat{\phi}_j = \tau_j^- (s) \tag{18a}$$

$$\text{at } x = 0.5a \quad \hat{\phi}_j = \alpha_j^+ (s) \quad \text{or} \quad \pi_j \hat{\phi}_j = \tau_j^+ (s) \tag{18b}$$

for $j = 1, 2, \ldots, N$, where $\alpha_j^\pm (s)$ are the prescribed displacements at the nodes.

Equations (16) and (18) are rewritten in a state equation form

$$\frac{\partial}{\partial x} \{\eta(x, s)\} = [\mathbf{F}(s)] \{\eta(x, s)\} + \{\mathbf{p}(x, s)\} \tag{19a}$$

$$[\mathbf{M}_b(s)] \{\eta(-0.5a, s)\} + [\mathbf{N}_b(s)] \{\eta(0.5a, s)\} = \{\gamma_b(s)\} \tag{19b}$$

where the state variable vector is defined by

$$\{\eta\} = \left\{ \hat{\phi}_1 \quad \frac{\partial}{\partial x} \hat{\phi}_1 \quad \hat{\phi}_2 \quad \frac{\partial}{\partial x} \hat{\phi}_2 \quad \ldots \quad \hat{\phi}_N \quad \frac{\partial}{\partial x} \hat{\phi}_N \right\}^{\mathrm{T}} \in C^{2N} \tag{20}$$

the state-space matrix $[\mathbf{F}(s)]$ is composed of the elements of $[\mathbf{A}_1]$ and $[\mathbf{A}_2(s)]$ defined in (16), the boundary matrices $[\mathbf{M}_b(s)]$ and $[\mathbf{N}_b(s)]$ consist of the coefficients of π_j given in (18), the external force vector $\{\mathbf{p}(x, s)\}$ contains the elements of $\{\mathbf{Q}_{ej}(x, s)\}$, and the boundary disturbance vector $\{\gamma_b(s)\}$ has the entries like $\alpha_j^\pm (s)$ and $\tau_j^\pm (s)$. For systematic construction of these matrices and vectors, refer to Yang and Tan (1992).

The solution to the state-space equations (19) is obtained in exact and closed form (Yang and Tan, 1992)

$$\{\eta(x, s)\} = \int_{-0.5a}^{0.5a} [\mathbf{G}(x, \xi, s)] \{\mathbf{p}(\xi, s)\} \, \mathrm{d}\xi + [\mathbf{H}(x, s)] \{\gamma_b(s)\} \tag{21}$$

where the $2N$ by $2N$ matrix Green's functions

$$[\mathbf{G}(x, \xi, s)] = \begin{cases} [\mathbf{H}(x, s)][\mathbf{M}_b(s)] e^{-[\mathbf{F}(s)](0.5a + \xi)}, & \xi \leqslant x \\ -[\mathbf{H}(x, s)][\mathbf{N}_b(s)] e^{[\mathbf{F}(s)](0.5a - \xi)}, & \xi > x \end{cases} \tag{22a}$$

$$[\mathbf{H}(x, s)] = e^{[\mathbf{F}(s)]x} ([\mathbf{M}_b(s)] e^{-0.5a[\mathbf{F}(s)]} + [\mathbf{N}_b(s)] e^{0.5a[\mathbf{F}(s)]})^{-1}. \tag{22b}$$

The $[\mathbf{G}(x, \xi, s)]$ and $[\mathbf{H}(x, s)]$ are called the strip distributed transfer functions of the rectangular region. By (22a), the evaluation of the integral in (21) depends on the evaluation of the integral $\int \exp\{-[\mathbf{F}(s)]\xi\} \{p(\xi, s)\} \, \mathrm{d}\xi$, which, in most cases, can be obtained by exact and closed-form quadrature without numerical integration (Yang, 1994). The state variable vector, once determined, directly gives the strains and stresses without the need to differentiate the nodal line displacement functions.

The transfer function formulation provides a systematic and efficient way to predict the static and dynamic response of the rectangular region under various loads and boundary conditions. The static displacements and strains are given by (21) with $s = 0$:

$$\{\eta(x,0)\} = \int_{-0.5a}^{0.5a} [\mathbf{G}(x,\xi,0)]\{\mathbf{p}(\xi,0)\}\,\mathrm{d}\xi + [\mathbf{H}(x,0)]\{\gamma_b(0)\}. \tag{23}$$

For the region under a harmonic excitation of frequency ω, its dynamic response is obtained by setting $s = i\omega$, $i = \sqrt{-1}$, in (21).

For free vibration of the elastic region, the natural frequencies ω_k are the roots of the transcendental characteristic equation

$$\det([\mathbf{M}_b(i\omega_k)]\mathrm{e}^{-0.5a[\mathbf{F}(i\omega_k)]} + [\mathbf{N}_b(i\omega_k)]\mathrm{e}^{0.5a[\mathbf{F}(i\omega_k)]}) = 0, \quad k = 1,2,\ldots \tag{24}$$

where $i = \sqrt{-1}$. The eigenfunction (mode shape) corresponding to ω_k is obtained by first determining

$$\eta = \mathrm{e}^{\mathbf{F}(i\omega_k)x}\psi, \quad x \in (-0.5a, 0.5a) \tag{25}$$

where the non-zero vector $\psi \in \mathrm{C}^{2N}$ satisfies

$$([\mathbf{M}_b(i\omega_k)]\mathrm{e}^{-0.5a[\mathbf{F}(i\omega_k)]} + [\mathbf{N}_b(i\omega_k)]\mathrm{e}^{0.5a[\mathbf{F}(i\omega_k)]})\psi = 0 \tag{26}$$

and then, substituting $\hat{\phi}_i(x, i\omega_k)$ of $\{\eta\}$ back into (5).

3. ASSEMBLY OF MULTIPLE RECTANGULAR SUBREGIONS

The 2-D elastic region Ω in consideration is composed of NR rectangular subregions Ω_j, $j = 1, 2, \ldots, \mathrm{NR}$. Two examples are shown in Figs (3a) and 3(b) where a U-shaped region is viewed as an assemblage of three rectangular subregions Ω_1 (ABCIJA), Ω_2 (CDHIC) and Ω_3 (DEFGHD), and a more complicated region is decomposed into seven rectangular subregions. While decomposition of a region may take different ways to avoid difficulties in assembly of subregions, nodal lines are defined such that the nodes (ends) of any nodal line are never connected to the interior points of other nodal lines. This means that all nodal lines should be aligned in one direction.

For each subregion, there are two types of nodes: (a) inter-connecting points where the neighboring subregions are inter-connected, and (b) boundary nodes where boundary conditions are prescribed; see Fig. 3(a) for instance. The region Ω is assembled from the subregions by imposing displacement continuity and force balance at those nodes where the subregions are inter-connected. In the sequel, the superscript i refers to the ith subregion Ω_i.

Consider subregion Ω_i. Let the length of the strips be a_i so that the nodal line displacements are defined in the domain $-0.5a_i \leqslant x \leqslant 0.5a_i$. Assume that there are N_c^i

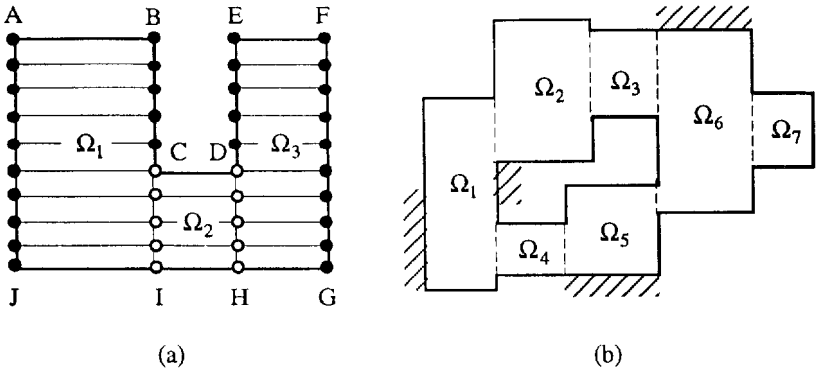

Fig. 3. Two dimensional regions composed of rectangular subregions: (a) a U-shaped region, ○—inter-connecting nodes, ●—boundary nodes; (b) a region composed of seven subregions.

unknown displacements at the inter-connecting nodes, which are denoted by the vector $\{\hat{\phi}_c^i(s)\} \in C_c^{N_c^i}$, and N_b^i boundary conditions specified at the boundary nodes, where the boundary disturbances are represented by the vector $\{\gamma_b^i(s)\} \in C_b^{N_b^i}$. The state variable vector of the subregion can be expressed in terms of the displacements at the inter-connecting nodes by viewing $\{\hat{\phi}_c^i(s)\}$ as the boundary disturbances; namely by (21),

$$\{\eta^i(x,s)\} = \{\eta_{cb}^i(x,s)\} + [\mathbf{H}_\phi^i(x,s)]\{\hat{\phi}_c^i(s)\}. \tag{27}$$

where

$$\{\eta_{cb}^i(x,s)\} = \int_{0.5a}^{0.5a} [\mathbf{G}^i(x,\xi,s)]\{\mathbf{p}^i(\xi,s)\}\,\mathrm{d}\xi + [\mathbf{H}_b^i(x,s)]\{\gamma_b^i(s)\}$$

and

$$[\mathbf{H}_\phi^i(x,s) \quad \mathbf{H}_b^i(x,s)] = [\mathbf{H}^i(x,s)].$$

With the above representation, displacement continuity at the inter-connecting nodes is guaranteed.

Let $\{\mathbf{S}_c^i(s)\} \in C^{N_c^i}$ be the vector of the internal forces applied at the inter-connecting nodes by Ω_i. For the convenience in derivation, the locations of these nodes are symbolically expressed by x_c, which is either $-0.5a_i$ or $0.5a_i$. The internal forces at the inter-connecting nodes are given by

$$\{\mathbf{S}_c^i(s)\} = [\Pi_c^i]\eta(x_c,s) \tag{28}$$

where the matrix $[\Pi_c^i]$, which describes a stress-displacement relationship, is derivable from the operator $[\Pi_\phi]$ in (15). Thus, from (27) and (28)

$$\{\mathbf{S}_c^i(s)\} = -[\mathbf{K}_c^i(s)]\{\hat{\phi}_c^i(s)\} + \{\mathbf{q}_c^i(s)\} \tag{29}$$

with

$$[\mathbf{K}_c^i(s)] = -[\Pi_c^i][\mathbf{H}_\phi^i(x_c,s)], \quad \{\mathbf{q}_c^i(s)\} = [\Pi_c^i]\{\eta_{cb}^i(x_c,s)\}.$$

where $\{\mathbf{q}_c^i(s)\}$ represents the transmitted internal forces at the inter-connecting nodes due to the external loads and boundary disturbances.

Now introduce the global nodal displacement vector $\{\hat{\phi}_c(s)\}$ which is a collection of all the independent unknown displacements in $\{\hat{\phi}_c^i(s)\}$, $i = 1, 2, \ldots, \mathrm{NR}$. At the inter-connecting nodes, there are internal forces $[\mathbf{S}_c^i(s)]$ exerted by the subregions, and the external lumped forces, which are denoted by the global vector $\{\mathbf{q}_e(s)\}$. Force balance at those nodes leads to the global dynamic equilibrium equation

$$[\mathbf{K}_c(s)]\{\hat{\phi}_c(s)\} = \{\mathbf{q}(s)\} \equiv \{\mathbf{q}_c(s)\} + \{\mathbf{q}_e(s)\} \tag{30}$$

where the matrix $[\mathbf{K}_c(s)]$ and the vector $\{\mathbf{q}_c(s)\}$ are assembled from $[\mathbf{K}_c^i(s)]$ and $\{\mathbf{q}_c^i(s)\}$ of the subregions in the same way as in the finite element analysis. The $[\mathbf{K}_c(s)]$ and $\{\mathbf{q}(s)\}$ are the global stiffness matrix and nodal force vector, respectively.

Upon its formation, the global dynamic equilibrium equation is ready to be solved since the boundary conditions of the region Ω have been introduced at the subregion level. The global stiffness matrix is symmetric for $s = 0$, and $s = i\omega$ where $i = \sqrt{-1}$. Thus the linear algebra eqn (30) can be easily solved by standard methods. Substitution of the solution of (30) into (27) and (5) gives the semi-analytical prediction of the static and

dynamic response of the 2-D region. The natural frequencies ω_k of the elastic body can be determined from $\det[\mathbf{K}_c(i\omega_k)] = 0$.

4. STRIP DISPLACEMENT INTERPOLATION

Three types of shape functions are introduced for the strip displacement interpolation discussed in Section 2.1.

Linear displacement interpolation model (*LM*). The nodal line displacement vector of the jth strip is chosen as

$$\{\mathbf{U}_j(x,t)\} = \{\psi_j(x,t) \quad \psi_{j+1}(x,t)\}^{\mathrm{T}} \tag{31}$$

where

$$\{\psi_l(x,t)\} = \{u_l(x,t) \quad v_l(x,t)\}^{\mathrm{T}}, \quad l = j, j+1 \tag{32}$$

and no internal nodal line displacements are used. The shape functions are given by

$$[\mathbf{N}_u(y)] = [1-\xi \quad 0 \quad \xi \quad 0], \quad [\mathbf{N}_v(y)] = [0 \quad 1-\xi \quad 0 \quad \xi] \tag{33}$$

where $\xi = y/b_j$ with b_j being the width of the strip.

Quadratic displacement interpolation model (*QM*). In this model, an internal nodal line is introduced at the middle of a strip. The nodal line displacement vector of the jth strip is given by (4), with $\{\psi_j\}$ and $\{\psi_{j+1}\}$ given in (32), and $\{\lambda_j\}$ defined by

$$\{\lambda_j(x,t)\} = \{u(x, b_j/2, t) \quad v(x, b_j/2, t)\}^{\mathrm{T}}. \tag{34}$$

The corresponding shape functions are

$$\begin{aligned}[\mathbf{N}_u(y)] &= [1-3\xi+2\xi^2 \quad 0 \quad 4\xi-4\xi^2 \quad 0 \quad 2\xi^2-\xi \quad 0] \\ [\mathbf{N}_v(y)] &= [0 \quad 1-3\xi+2\xi^2 \quad 0 \quad 4\xi-4\xi^2 \quad 0 \quad 2\xi^2-\xi].\end{aligned} \tag{35}$$

Cubic displacement interpolation model (*CM*). The nodal line displacement vector of the jth strip is given by (31) with

$$\{\psi_l(x,t)\} = \{u_l(x,t) \quad v_l(x,t) \quad u_{yl}(x,t) \quad v_{yl}(x,t)\}^{\mathrm{T}}, \quad l = j, j+1 \tag{36}$$

where u_{yl} and v_{yl} are the derivatives $\partial u/\partial y$ and $\partial v/\partial y$ on the jth nodal line. No internal nodal line parameters are used in this model. The shape functions are

$$\begin{aligned}[\mathbf{N}_u(y)] &= [1-3\xi^2+2\xi^3 \quad 0 \quad b_j(\xi-2\xi^2+\xi^3) \quad 0 \quad 3\xi^2-2\xi^3 \quad 0 \quad b_j(-\xi^2+\xi^3) \quad 0] \\ [\mathbf{N}_v(y)] &= [0 \quad 1-3\xi^2+2\xi^3 \quad 0 \quad b_j(\xi-2\xi^2+\xi^3) \quad 0 \quad 3\xi^2-2\xi^3 \quad 0 \quad b_j(-\xi^2+\xi^3)].\end{aligned} \tag{37}$$

For each model, the stiffness and mass matrices defined in (8) are given in the Appendix.

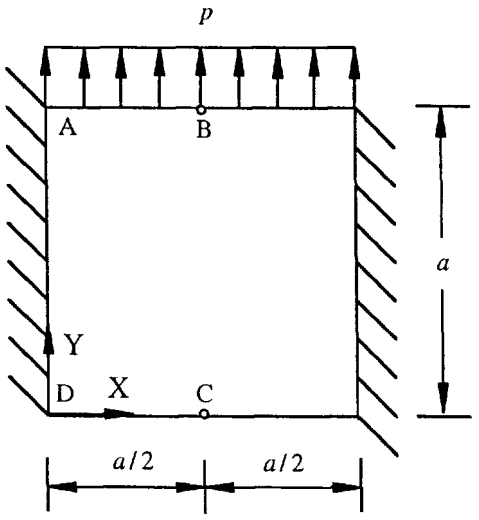

Fig. 4. A square region under a uniformly distributed load.

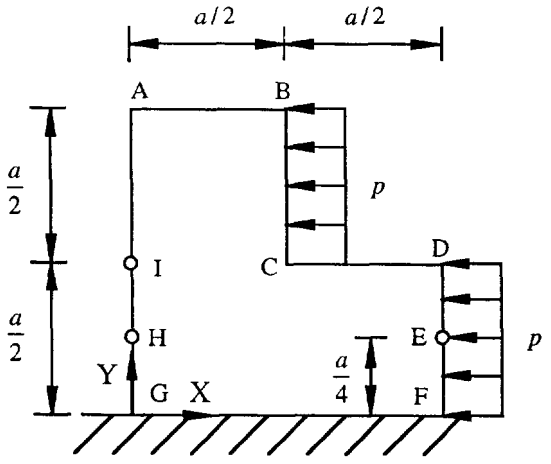

Fig. 5. An L-shaped region under uniformly distributed loads.

5. NUMERICAL RESULTS

The strip distributed transfer function method is illustrated on a square region (Fig. 4), and an L-shaped region (Fig. 5). Static displacements and stresses are predicted by the proposed method using the three models (LM, QM, and CM) developed in Section 4, and the results obtained are compared with those by the finite element method. Also, the natural frequencies of the L-shaped region in free vibration are calculated. The finite element simulation is done using a 4-node isoparametric element and an 8-node isoparametric element from the software COSMOS/M. While the proposed SDTFM is valid for anisotropic elasticity, for demonstrative purposes, only isotropic elastic material in the state of plane stress is considered in the numerical examples. The displacement and stress results are non-dimensionized by

$$\bar{u} = \frac{E}{1-\mu^2}u, \quad \bar{v} = \frac{E}{1-\mu^2}v, \quad \bar{\sigma}_x = \frac{\sigma_x}{p}, \quad \bar{\sigma}_y = \frac{\sigma_y}{p}, \quad \bar{\tau}_{xy} = \frac{\tau_{xy}}{p} \tag{38}$$

where p is a load parameter, E is Young's modulus, and μ is Poisson's ratio, which is 0.3 in all the calculations.

Table 1. Displacement and stresses at point B of the square (NS—number of strips)

Method		Mesh	$\bar{v}$	$\bar{\sigma}_x$	$\bar{\sigma}_y$
SDTFM	LM	$NS = 1$	0.6151	0.3499	0.5176
		2	0.6783	0.4999	0.7810
		4	0.7293	0.7617	0.9918
		8	0.7546	0.8640	1.0451
	QM	$NS = 1$	0.7027	0.6228	1.0282
		2	0.7470	0.8744	1.1186
		4	0.7635	0.8965	1.0565
		8	0.7665	0.8785	1.0153
	CM	$NS = 1$	0.7513	0.9029	1.1678
		2	0.7636	0.9017	1.0510
		4	0.7664	0.8748	1.0047
		8	0.7672	0.8740	1.0001
FEM	4-node element	2×2	0.7554	0.1483	0.9440
		4×4	0.7309	0.7367	0.8611
		8×8	0.7563	0.8398	0.9688
		16×16	0.7639	0.8648	0.9928
	8-node element	2×2	0.6954	0.7747	1.3920
		4×4	0.7548	0.8722	0.9788
		8×8	0.7643	0.8623	1.0020
		16×16	0.7666	0.8708	1.0020
		50×50	0.7675	0.8740	1.0000

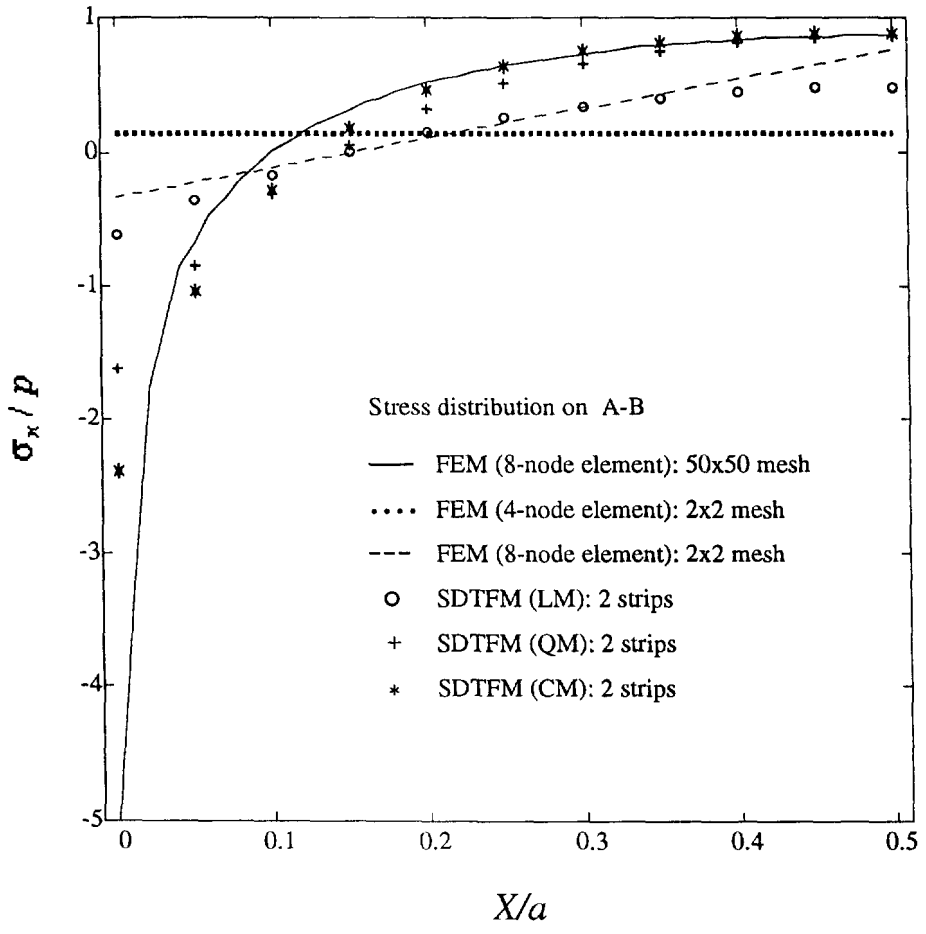

Fig. 6. Distribution of $\bar{\sigma}_x$ on A-B of the square region: SDTFM—2 strips; FEM—2×2 mesh.

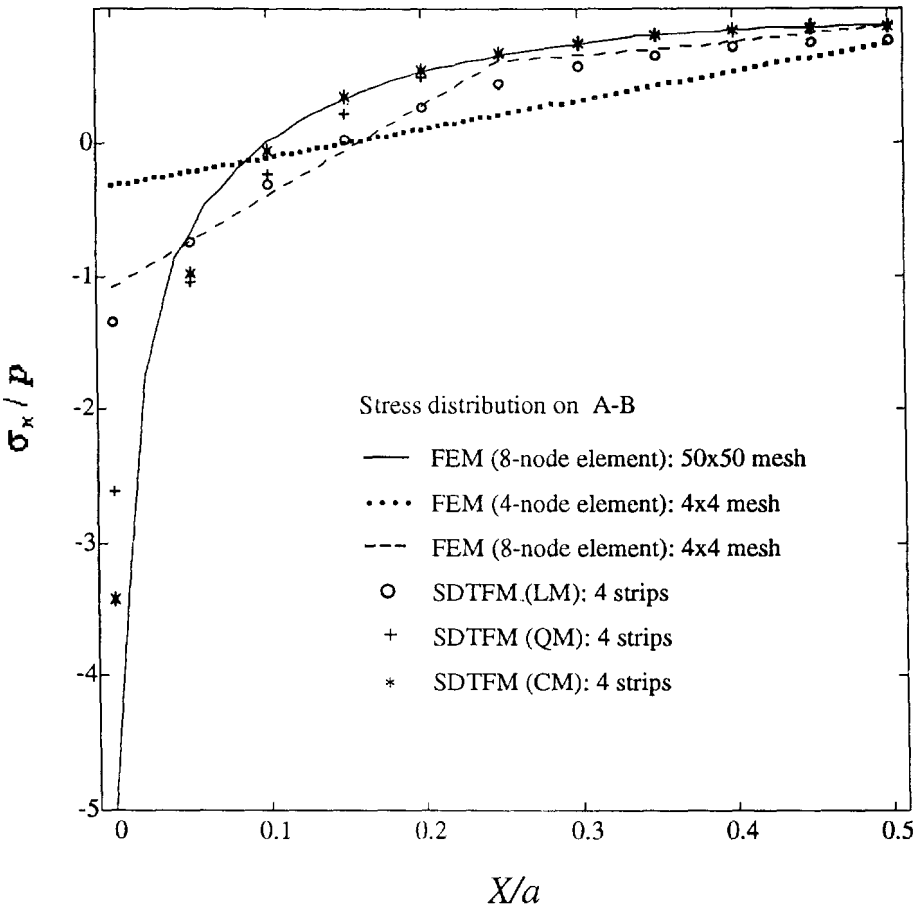

Fig. 7. Distribution of $\bar{\sigma}_x$ on A-B of the square region: SDTFM—4 strips; FEM—4 × 4 mesh.

Example 1: *static stresses of square region*

The square of side length a in Fig. 4 is clamped on both the vertical sides, and is subjected to a uniform load of magnitude p on the top side. In SDTFM, the square is divided into NS identical horizontal strips of width $b_j = a/NS$, whose longitudinal direction is in the X-direction. In the finite element analysis, the square is divided into an $N \times N$ mesh of identical square elements.

Table 1 shows the displacement $\bar{v}$ and normal stresses $\bar{\sigma}_x$ and $\bar{\sigma}_y$ at point B on the top side of the square. In the FEM category, the words "4-node element" and "8-node element" represent 4-node and 8-node isoparametric elements, respectively. All the three SDTFM models give accurate and fast-converging results. The LM with 8 strips is comparable to the 4-node element with an 8×8 mesh. The QM of 8 strips is more accurate than the 4-node element with a 16×16 mesh, and as accurate as the 8-node element with an 8×8 mesh. Higher accuracy is gained as the interpolation order increases: the CM with 8 strips is as good as the 8-node finite element with a 50×50 mesh (i.e., 2,500 elements).

The distributions of the stress $\bar{\sigma}_x$ along lines A-B and B-C are given in Figs 6–8 and Figs 9–11, respectively, for different meshes. Since the exact solution is not available for this problem, the prediction by the 8-node finite element with a 50×50 mesh is used as a reference solution, and plotted in each figure. It is apparent that the three SDTFM models yield much more accurate predictions than the FEM models, when the number NS of strips is the same as the N of the finite element mesh $N \times N$. The results obtained by the cubic SDTFM (CM) with 8 strips are almost the same as the reference solution. In addition, even with 2 strips the CM is more accurate than the 8-node element with an 8×8 mesh. Here the strip width is 4 times of the side length of the finite elements.

Notice that at point A of the square, the stress $\bar{\sigma}_x$ becomes singular. An 8×8 mesh is too coarse for the finite element models to describe the high gradient of the stress and much

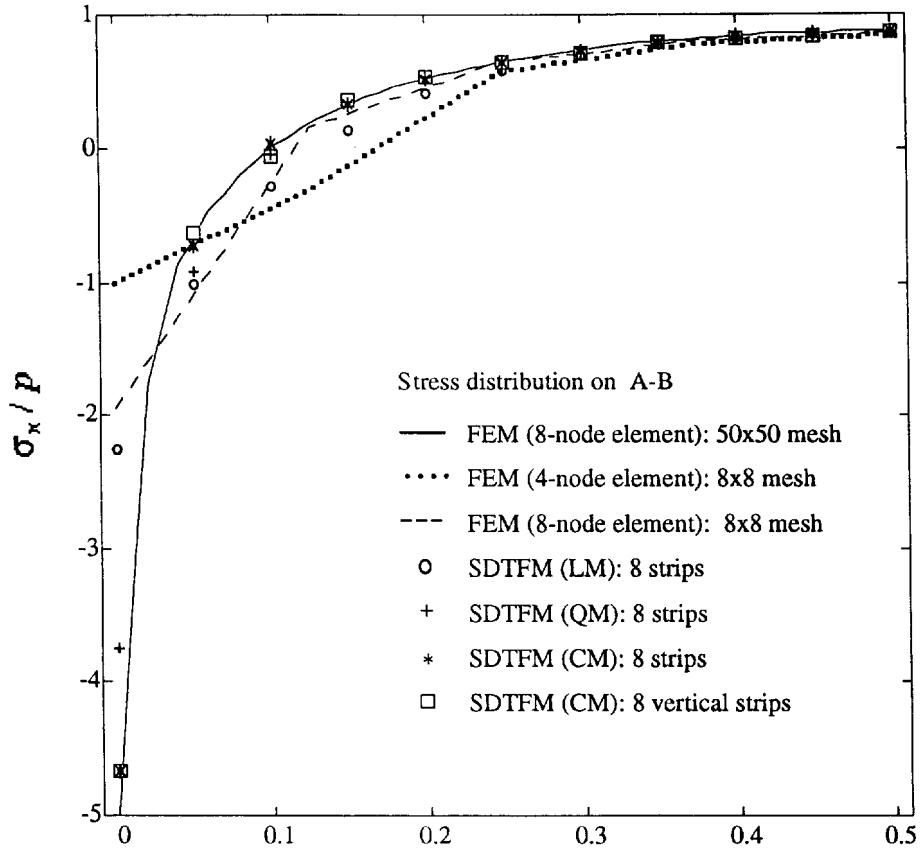

Fig. 8. Distribution of $\bar{\sigma}_x$ on A-B of the square region: SDTFM—8 strips; FEM—8 × 8 mesh.

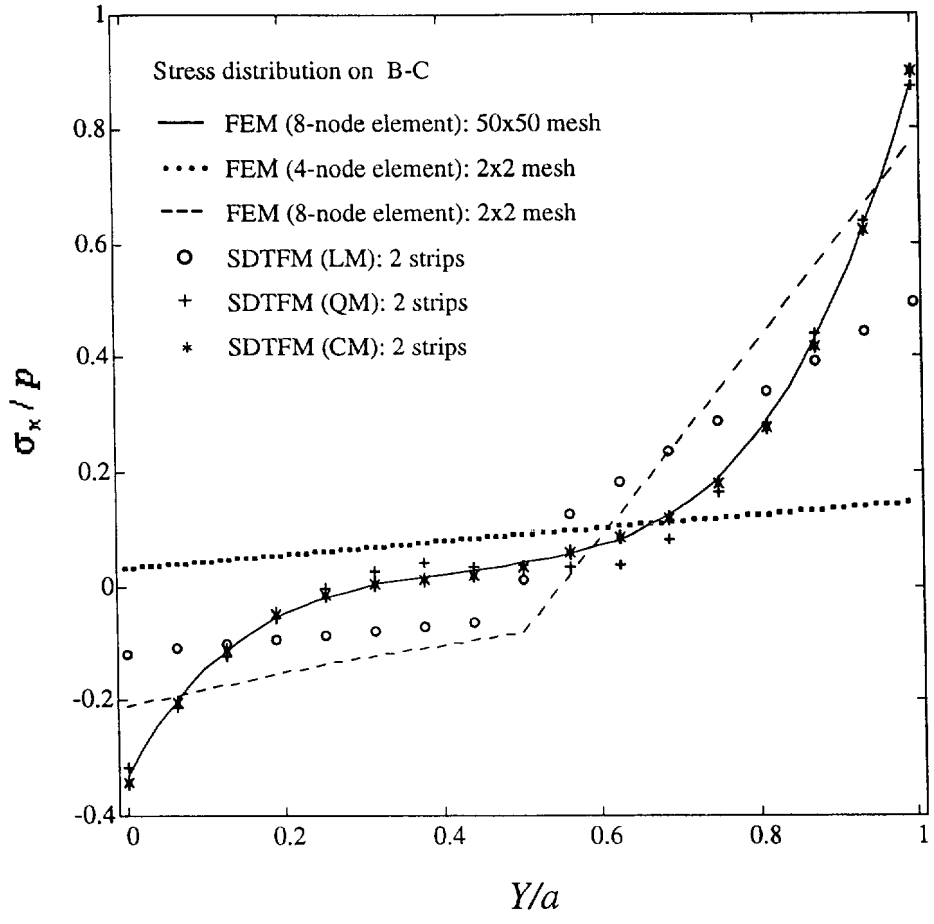

Fig. 9. Distribution of $\bar{\sigma}_x$ on B-C of the square region: SDTFM—2 strips; FEM—2 × 2 mesh.

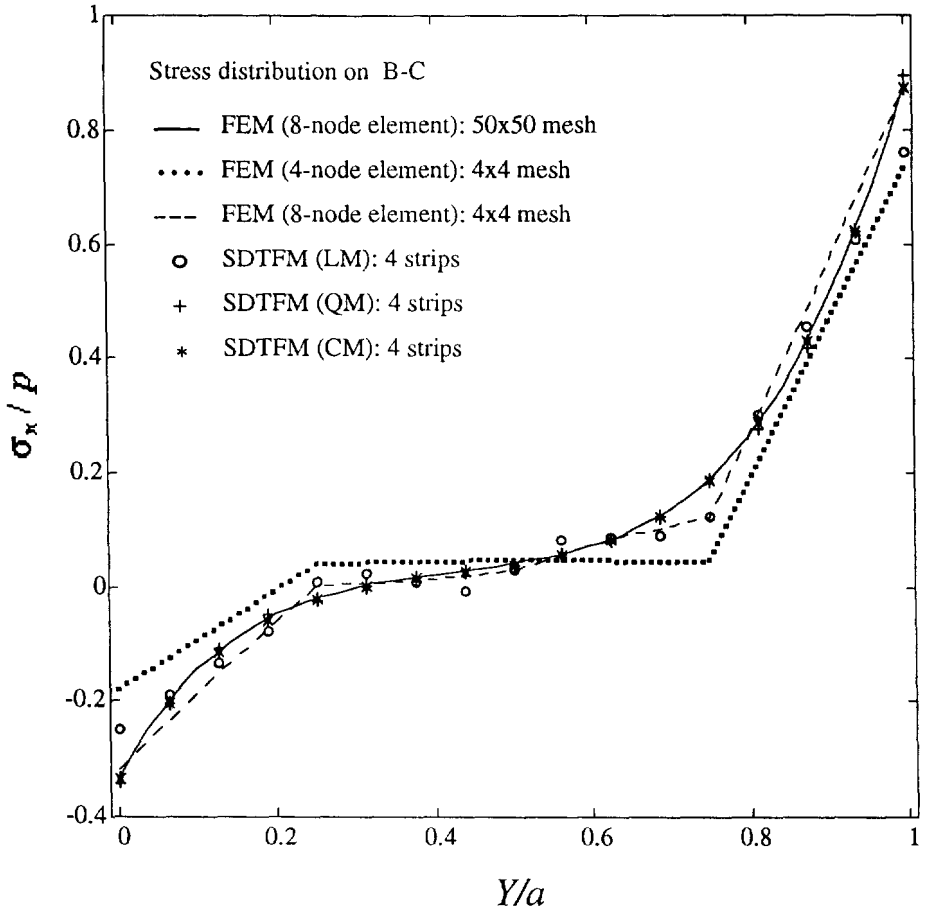

Fig. 10. Distribution of $\bar{\sigma}_x$ on B-C of the square region: SDTFM—4 strips; FEM—4 × 4 mesh.

more elements are needed. On the other hand, with just 8 strips, the CM of SDTFM gives a pretty good profile of the stress distribution near the point; see Fig. 8.

To check the consistence of the proposed method, $\bar{\sigma}_x$ on line A-B is re-calculated using 8 vertical strips, and plotted against that predicted by 8 horizontal strips; see Fig. 8. The stress estimated by the vertical strips is slightly different from that by the horizontal strips at certain points where the curvature of the stress distribution is relatively large. The difference, while not significant, is obviously due to the discretization of the strip displacements in the direction of A-B. However, with the exact nodal line displacements determined at the nodes on line A-B, the vertical strips still faithfully present the singularity of the stress at point A. This insensitivity of the proposed method to strip orientation is also seen in Example 2 (Figs 12 and 16).

Example 2: static stresses of L-shaped region

The L-shaped region in Fig. 5 is clamped at the bottom, and subjected to a uniform in-plane load of magnitude p on its two right sides. In the transfer function synthesis, the region is divided into two subregions: subregion 1, Ω_1 = ICDEFGHI; and subregion 2, Ω_2 = ABCIA. The subregions are divided into identical vertical strips, with their longitudinal direction in the Y-direction. Two subregions are inter-connected at the nodes on line I-C. Since Ω_1 is twice as large as Ω_2, if Ω_2 has NS strips, Ω_1 has $2NS$ strips, and the whole region has total $2NS+NS$ strips. The finite element meshing follows a similar pattern: Ω_2 has $N \times N$ identical square elements, Ω_1 has $2N \times N$ elements, and the whole region has $2N \times N + N \times N$ elements.

The distributions of the stresses $\bar{\sigma}_y$ and $\bar{\sigma}_x$ on different lines of the region are plotted in Figs 12–16, where the strip number $2NS+NS$ and the finite element mesh $2N \times N + N \times N$ bear the same meaning as explained in the previous paragraph. As a reference, the solution

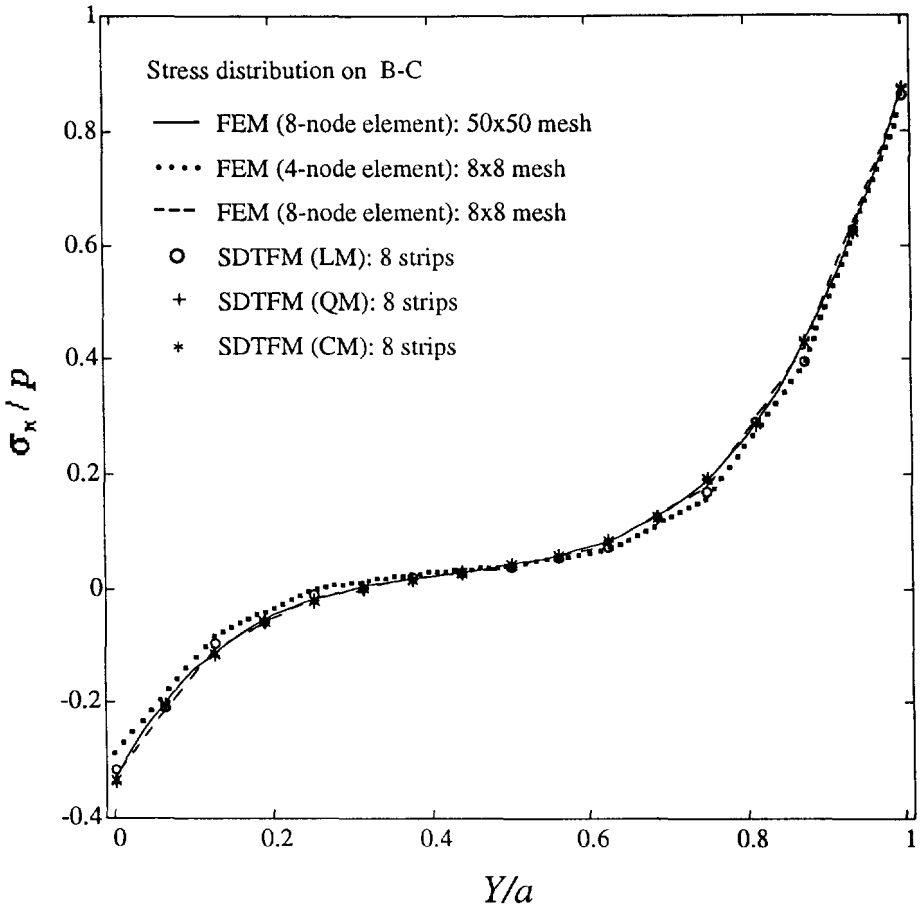

Fig. 11. Distribution of $\bar{\sigma}_x$ on B-C of the square region: SDTFM—8 strips; FEM—8×8 mesh.

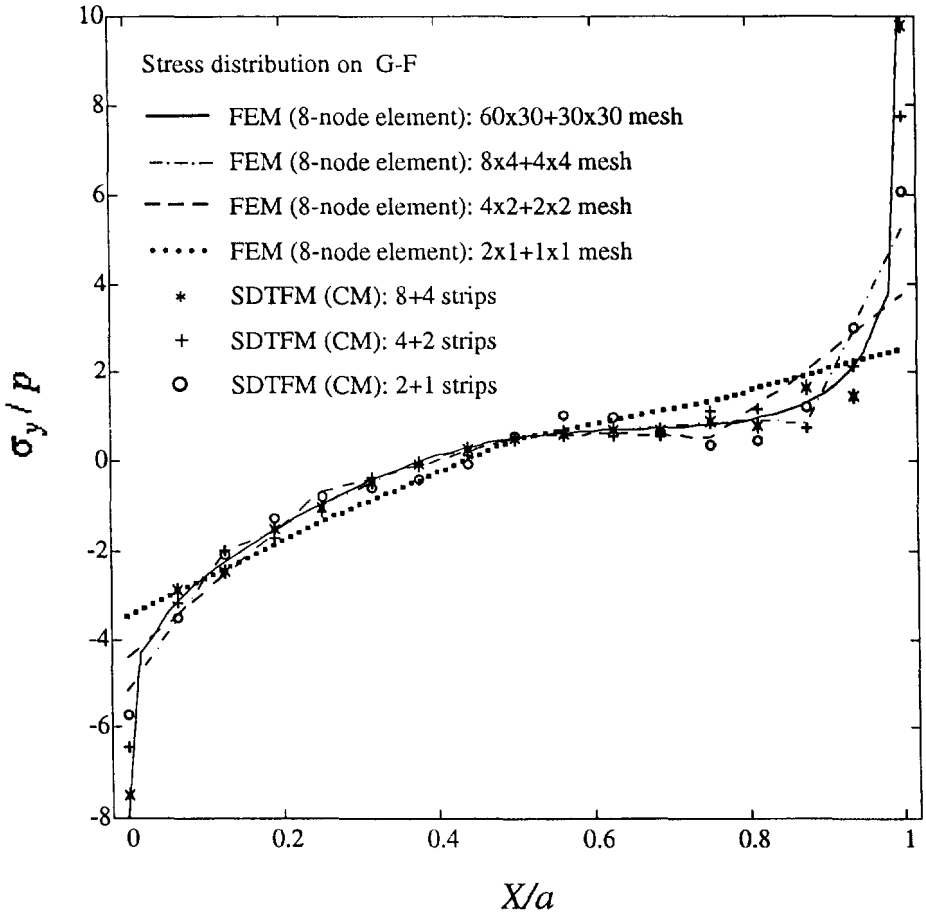

Fig. 12. Distribution of $\bar{\sigma}_y$ on G-F of the L-shaped region.

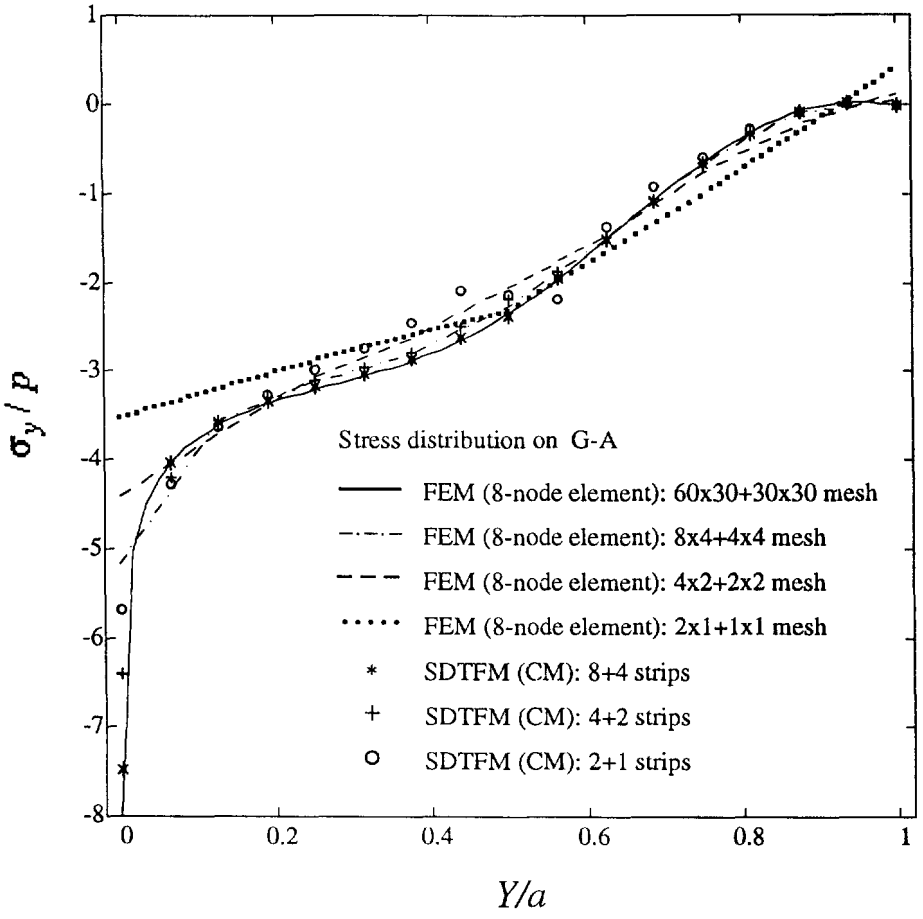

Fig. 13. Distribution of $\bar{\sigma}_y$ on G-A of the L-shaped region.

by the 8-node isoparametric element with a mesh of $60 \times 30 + 30 \times 30$ (total 2,700 elements) is provided in each figure. Again the high accuracy and fast convergence of the SDTFM solutions are seen, especially in the prediction of stress distributions of high gradient.

Example 3: *natural frequencies of L-shaped region*

The same L-shaped region in Example 2 is in free vibration. Shown in Table 2 are the first 10 natural frequencies of the continuum, computed by the quadratic SDTFM (QM), and the 8-node finite element. The natural frequencies ω_k of the elastic region are non-dimensionized by

$$\bar{\omega}_k = \omega_k a \sqrt{\frac{12\rho h(1-\mu^2)}{E}}. \tag{39}$$

The prediction by the finite element method with a $70 \times 35 + 35 \times 35$ mesh (total 3,675 elements) serves as a reference solution. For each case of FEM or SDTFM mesh, there is a column of numbers under the symbol ε (%), which stands for the percentage deviation of the computed results from the reference solution.

With just 12 (8+4) strips, the proposed method gives accurate predictions, with the maximum deviation from the reference solution less than 0.4%. Note that the deviation becomes smaller for higher-mode frequencies. With 6 (4+2) strips, the maximum deviation is less than 1.5%, which is better than that of the result obtained using 48 finite elements. Even 3 (2+1) strips can have an acceptable maximum deviation of 5.7%. On the other hand, fewer finite elements would lead to poor accuracy in the predicted frequencies, as in the case of 12 elements. Since the quadratic model (QM) of SDTFM already has enough

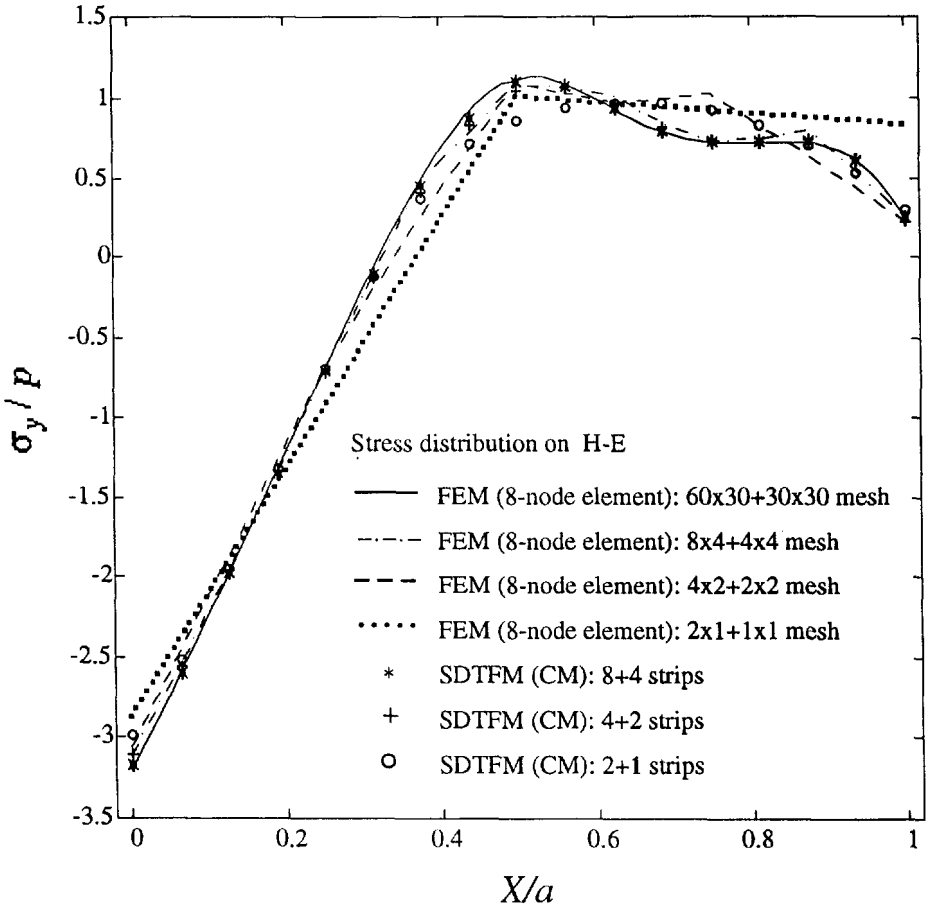

Fig. 14. Distribution of $\bar{\sigma}_y$ on H-E of the L-shaped region.

precision, the more accurate cubic model (CM) is not necessary in this example. All these indicate that SDTFM is useful for analysis of high-frequency dynamics of complex elastic bodies.

Some observations from the numerical simulation are in order. If the strip width is equal to the side length of finite elements, the SDTFM results have much higher precision than those by FEM. This advantage is most obvious when the mesh is coarse or the stress gradient is high. Among the three SDTFM models, the cubic interpolation model (CM) has the highest precision. This model maintains continuity of strains and stresses across nodal lines, and does not need averaging the strains and stresses of adjacent strips on their mutual boundaries (nodal lines). If strain or stress discontinuity does exist across a nodal line, however, the model should be carefully used. On the other hand, the linear interpolation model (LM) and the quadratic interpolation model (QM) have discontinuity in strain and stress across nodal lines. In this case, the strain and stress values on a nodal line are taken as the average of those of the two adjacent strips on their mutual boundary, i.e., the nodal line. The numerical results show that the difference between the stresses of the two adjacent strips on their boundary nodal line is small for the quadratic model (QM), even when the strip mesh is coarse.

6. DISCUSSION

Some important features of SDTFM can be clearly seen by comparing it with FEM, series solution methods (Galerkin, Ritz and assumed-modes methods), and the finite strip method. Figure 17 shows the different strategies of these methods in describing the response of a 2-D rectangular region in the X- and Y-directions. The finite strip method can be

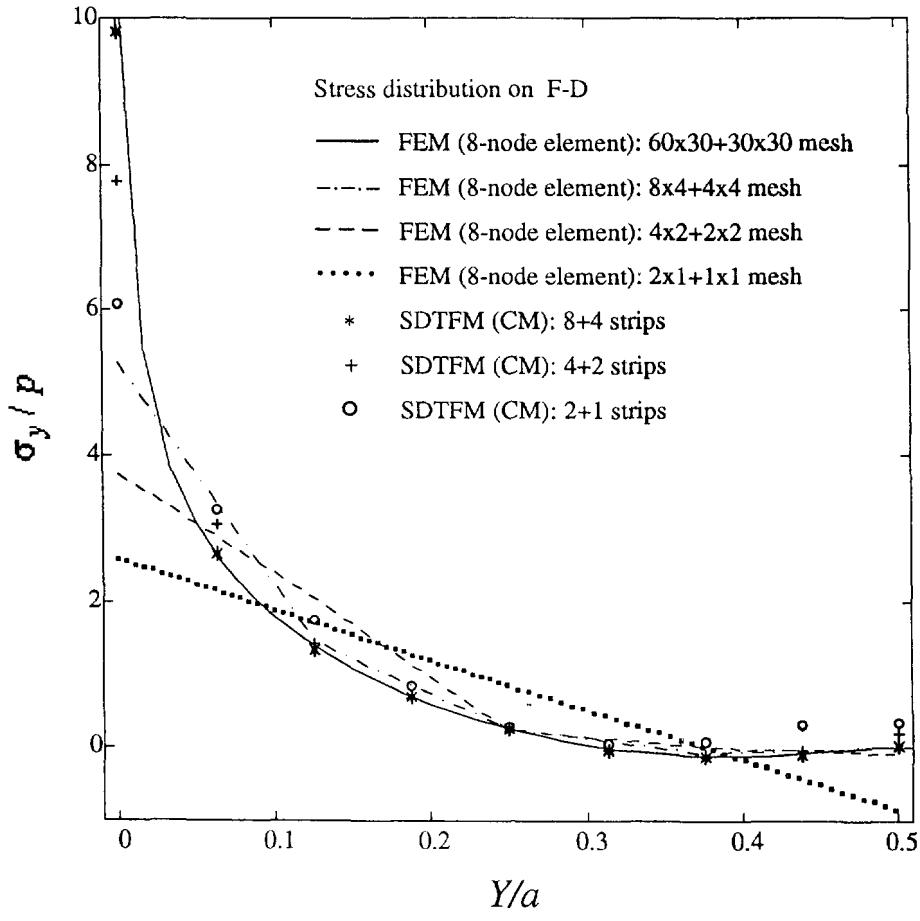

Fig. 15. Distribution of $\bar{\sigma}_y$ on F-D of the L-shaped region.

viewed as a combination of FEM and series solution method, while the proposed SDTFM is a combination of FEM and exact analytical solution approach.

Both series solution methods and the finite strip method adopt series of comparison or admissible functions, which are usually selected on a problem-by-problem basis, and may be difficult to find even for some simple regions. On top of that, since the number of terms in a series has to be large enough to gain necessary accuracy, in general, there is no one-to-one mapping between the coefficients in the series and the displacements of the region at the pre-selected boundary nodes. Because of these, it is difficult for series solution methods and the finite strip method to model multi-body branched regions with mixed boundary conditions, like the one shown in Fig. 3(b). Of course, one may fix the number of terms in the series so as to render subregions or strips being able to be assembled at boundary nodes. Doing so, however, will change the original format of infinite series solutions into finite element interpolation by continuous functions, which needs a lot more subregions or much shorter strips, in order to maintain the same accuracy level.

The finite element method has no such a problem: as a rule, the number of terms in the element interpolation functions always matches the number of the element nodal parameters. Nevertheless, given nodes, a large number of nodal parameters may impose too strong continuity on the mutual boundaries of elements. So, the accuracy of FEM is usually achieved by highly dense meshes.

The proposed SDTFM is fundamentally different from series solution methods and the finite strip method in three major aspects: (i) SDTFM gives exact closed-form solutions (nodal line displacements) in the strip longitudinal direction; (ii) SDTFM does not need to select particular functions for any given boundary conditions; and (iii) SDTFM uniquely expresses the response of subregions by the displacements at their boundary nodes. While only rectangular subregions are considered here, the strip distributed transfer function

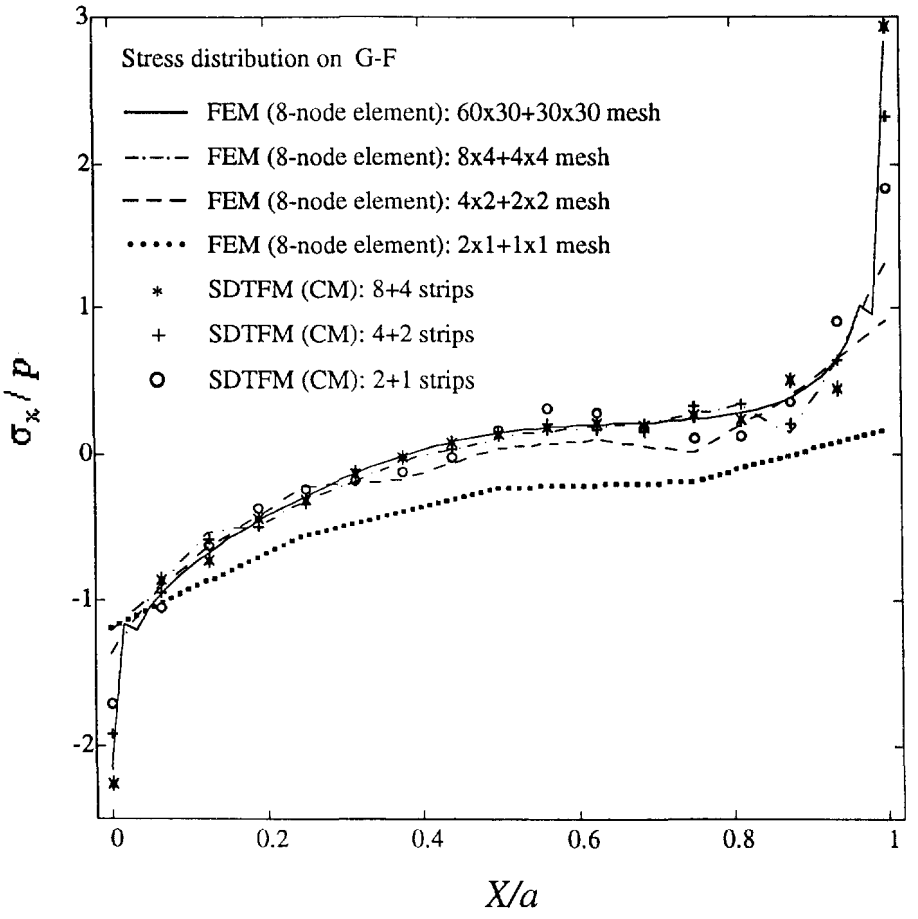

Fig. 16. Distribution of $\bar{\sigma}_x$ on G-F of the L-shaped region.

Table 2. Natural frequencies of an L-shaped elastic region

	SDTFM 2+1 strips		SDTFM 4+2 strips		SDTFM 8+4 strips		FEM 12 elements		FEM 48 elements		FEM 3.675 elements
k	$\bar{\omega}_k$	ε (%)	$\bar{\omega}_k$	ε (%)	$\bar{\omega}_k$	ε (%)	$\bar{\omega}_k$	ε (%)	$\bar{\omega}_k$	ε (%)	
1	2.3809	3.70	2.3285	1.42	2.3030	0.31	2.3375	1.81	2.3185	0.98	2.2959
2	5.7999	3.54	5.6453	0.77	5.6173	0.27	5.5395	−1.11	−5.6001	−0.03	5.6019
3	6.0142	0.76	5.9187	0.21	5.9187	0.21	5.9889	0.33	5.9763	0.12	5.9690
4	10.089	3.55	9.8402	0.99	9.7751	0.32	9.4712	−2.79	9.6937	−0.51	9.7434
5	11.943	3.12	11.641	0.51	11.591	0.08	11.343	−2.06	11.528	−0.46	11.582
6	14.624	5.67	13.959	0.87	13.856	0.12	13.275	−4.08	13.691	−1.07	13.839
7	15.033	5.04	14.419	0.75	14.324	0.08	14.009	2.12	14.232	−0.56	14.313
8	16.475	4.72	15.817	0.55	15.746	0.09	15.456	−1.75	15.703	−0.18	15.731
9	17.105	3.44	16.714	1.08	16.563	0.16	15.662	−5.29	16.398	−0.84	16.536
10	19.392	1.77	19.107	0.28	19.070	0.08	16.121	−15.4	18.112	−4.94	19.055

modeling is valid for elastic bodies of other shapes (Yang and Zhou, 1995). These features enable SDTFM to synthesize elastic regions of complex geometry and boundary conditions.

As shown in the numerical examples, the proposed SDTFM delivers much more accurate solutions than FEM. Two good reasons for this high accuracy of SDTFM are: (a) exact, closed-form analytical solution for nodal line displacements; and (b) determination of strain/stress components by the state variable vector given in (20), without differentiation of the nodal line displacements. Another advantage of SDTFM is that only the unknown displacements at those inter-connecting nodes (see Fig. 3(a)) are needed in

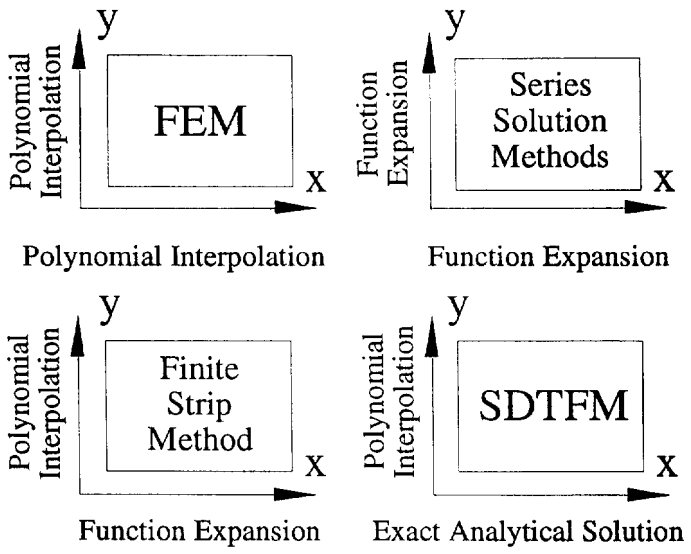

Fig. 17. Comparison of SDTFM with existing methods.

the global dynamic equilibrium equation (30). This automatic condensation, along with modeling by subregions, leads to a minimum number of unknowns to be determined.

7. CONCLUSIONS

The strip distributed transfer function method has been presented for static and dynamic analysis of two-dimensional elasticity problems. The thrust of the method is that it is flexible in dealing complex elastic regions, and at the same time delivers highly accurate solutions. By providing closed-form, semi-exact solutions, the proposed SDTFM is much more accurate than the finite element method, especially in predicting high-gradient stresses and high-frequency dynamics. Therefore, by SDTFM, tremendous data storage can be saved, and real-time computation for large-scale elastic systems is realizable.

The proposed method does not depend on series expansion of strip displacement functions, and selection of particular functions for specific boundary conditions. For an elastic subregion with any given boundary conditions, the method finds the exact solution of the dynamic equilibrium equation governing the nodal line displacements. Through use of the strip distributed transfer functions, the response of a subregion can be systematically represented by the displacements at its boundary nodes, just like in finite element analysis. Furthermore, SDTFM does not need increased computer memory to deal with concentrated loads, pointwise constraints, and abrupt changes in geometric and material properties. Accordingly, SDTFM is more capable of synthesizing elastic regions of complex geometry and boundary conditions than many methods that are based on continuous function expansion.

While the current work is focused on analysis of 2-D elastic bodies composed of rectangular subregions, the basic concepts of SDTFM presented in this paper are applicable to places, shells, and membranes consisting of subregions of different shapes, and certainly 3-D elastic bodies. Further development of this method is under way (Zhou and Yang, 1995; Yang and Zhou, 1995; Yang and Park, 1995). It is believed that the semi-analytical method proposed herein will become a useful tool for modeling and analysis of complex flexible structures, and other distributed parameter systems.

Acknowledgments—The work was partially supported by the US Army Research Office. The numerical simulation for Example 3 in Section 5 was conducted by Mr D.-H. Park. Also, the authors wish to acknowledge the anonymous reviewers for the helpful suggestions and comments with the presentation.

REFERENCES

Cheung, Y. K. (1976). *Finite Strip Method in Structural Analysis*. Pergamon Press, Oxford.
Yang, B. (1989). Active vibration control of axially moving materials. Ph.D. dissertation, UC Berkeley, California.
Yang, B. (1992). Transfer functions of constrained/combined one-dimensional continuous dynamic systems. *J. Sound Vibration* **156,** 425–443.
Yang, B. (1994). Distributed transfer function analysis of complex distributed systems. *ASME J. Appl. Mech.* **61,** 84–92.
Yang, B. and Park, D.-H. (1995). A prism distributed transfer function method for analysis of three-dimensional elastic bodies. To be submitted.
Yang, B. and Tan, C. A. (1992). Transfer functions of one dimensional distributed parameter systems. *ASME J. Appl. Mech.* **59,** 1009–1014.
Yang, B. and Zhou, J. (1995). Strip distributed transfer function analysis of circular and sectorial plates. *J. Sound Vibr.*
Zhou, J. and Yang, B. (1995). Strip distributed transfer function method for analysis of plates. *Int. J. Num. Meth. Engng* (in press).
Zienkiewicz, O. C. and Taylor, R. L. (1989). *The Finite Element Method* (4th ed.) McGraw-Hill Book Company, New York.

APPENDIX: STIFFNESS AND MASS MATRICES

Linear displacement interpolation model (LM)

$$[\mathbf{k}'_{11}] = \frac{b_j h}{6}\begin{bmatrix} 2C_{11} & 2C_{16} & C_{11} & C_{16} \\ 2C_{16} & 2C_{66} & C_{16} & C_{66} \\ C_{11} & C_{16} & 2C_{11} & 2C_{16} \\ C_{16} & C_{66} & 2C_{16} & 2C_{66} \end{bmatrix}, \quad [\mathbf{k}'_{01}] = \frac{h}{2}\begin{bmatrix} -C_{16} & -C_{66} & -C_{16} & -C_{66} \\ -C_{12} & -C_{26} & -C_{12} & -C_{26} \\ C_{16} & C_{66} & C_{16} & C_{66} \\ C_{12} & C_{26} & C_{12} & C_{26} \end{bmatrix}$$

$$[\mathbf{k}'_{00}] = \frac{h}{b_j}\begin{bmatrix} C_{66} & C_{26} & -C_{66} & -C_{26} \\ C_{26} & C_{22} & -C_{26} & -C_{22} \\ -C_{66} & -C_{26} & C_{66} & C_{26} \\ -C_{26} & -C_{22} & C_{26} & C_{22} \end{bmatrix}, \quad [\mathbf{m}'] = \frac{\rho h b_j}{6}\begin{bmatrix} 2 & 0 & 1 & 0 \\ 0 & 2 & 0 & 1 \\ 1 & 0 & 2 & 0 \\ 0 & 1 & 0 & 2 \end{bmatrix}.$$

Quadratic displacement interpolation model (QM)

$$[\mathbf{k}'_{11}] = \frac{b_j h}{30}\begin{bmatrix} 4C_{11} & 4C_{16} & 2C_{11} & 2C_{16} & -C_{11} & -C_{16} \\ 4C_{16} & 4C_{66} & 2C_{16} & 2C_{66} & -C_{16} & -C_{66} \\ 2C_{11} & 2C_{16} & 16C_{11} & 16C_{16} & 2C_{11} & 2C_{16} \\ 2C_{16} & 2C_{66} & 16C_{16} & 16C_{66} & 2C_{16} & 2C_{66} \\ -C_{11} & -C_{16} & 2C_{11} & 2C_{16} & 4C_{11} & 4C_{16} \\ -C_{16} & -C_{66} & 2C_{16} & 2C_{66} & 4C_{16} & 4C_{66} \end{bmatrix}$$

$$[\mathbf{k}'_{01}] = \frac{h}{6}\begin{bmatrix} -3C_{16} & -3C_{66} & -4C_{16} & -4C_{66} & C_{16} & C_{66} \\ -3C_{12} & -3C_{26} & -4C_{12} & -4C_{26} & C_{12} & C_{26} \\ 4C_{16} & 4C_{66} & 0 & 0 & -4C_{16} & -4C_{66} \\ 4C_{12} & 4C_{26} & 0 & 0 & -4C_{12} & -4C_{26} \\ -C_{16} & -C_{66} & 4C_{16} & 4C_{66} & 3C_{16} & 3C_{66} \\ -C_{12} & -C_{26} & 4C_{12} & 4C_{26} & 3C_{12} & 3C_{26} \end{bmatrix}$$

$$[\mathbf{k}'_{00}] = \frac{h}{3b_j}\begin{bmatrix} 7C_{66} & 7C_{26} & -8C_{66} & -8C_{26} & C_{66} & C_{26} \\ 7C_{26} & 7C_{22} & -8C_{26} & -8C_{22} & C_{26} & C_{22} \\ -8C_{66} & -8C_{26} & 16C_{66} & 16C_{26} & -8C_{66} & -8C_{26} \\ -8C_{26} & -8C_{22} & 16C_{26} & 16C_{22} & -8C_{26} & -8C_{22} \\ C_{66} & C_{26} & -8C_{66} & -8C_{26} & 7C_{66} & 7C_{26} \\ C_{26} & C_{22} & -8C_{26} & -8C_{22} & 7C_{26} & 7C_{22} \end{bmatrix}$$

$$[\mathbf{m}'] = \frac{\rho h b_j}{30}\begin{bmatrix} 4 & 0 & 2 & 0 & -1 & 0 \\ 0 & 4 & 0 & 2 & 0 & -1 \\ 2 & 0 & 16 & 0 & 2 & 0 \\ 0 & 2 & 0 & 16 & 0 & 2 \\ -1 & 0 & 2 & 0 & 4 & 0 \\ 0 & -1 & 0 & 2 & 0 & 4 \end{bmatrix}.$$

Cubic displacement interpolation model (CM)

$$[\mathbf{k}_{11}^j] = \frac{b_j h}{420}\begin{bmatrix}
156C_{11} & 156C_{16} & 22b_jC_{11} & 22b_jC_{16} & 54C_{11} & 54C_{16} & -13b_jC_{11} & -13b_jC_{16}\\
156C_{16} & 156C_{66} & 22b_jC_{16} & 22b_jC_{66} & 54C_{16} & 54C_{66} & -13b_jC_{16} & -13b_jC_{66}\\
22b_jC_{11} & 22b_jC_{16} & 4b_j^2C_{11} & 4b_j^2C_{16} & 13b_jC_{11} & 13b_jC_{16} & -3b_j^2C_{11} & -3b_j^2C_{16}\\
22b_jC_{16} & 22b_jC_{66} & 4b_j^2C_{16} & 4b_j^2C_{66} & 13b_jC_{16} & 13b_jC_{66} & -3b_j^2C_{16} & -3b_j^2C_{66}\\
54C_{11} & 54C_{16} & 13b_jC_{11} & 13b_jC_{16} & 156C_{11} & 156C_{16} & -22b_jC_{11} & -22b_jC_{16}\\
54C_{16} & 54C_{66} & 13b_jC_{16} & 13b_jC_{66} & 156C_{16} & 156C_{66} & -22b_jC_{16} & -22b_jC_{66}\\
-13b_jC_{11} & -13b_jC_{16} & -3b_j^2C_{11} & -3b_j^2C_{16} & -22b_jC_{11} & -22b_jC_{16} & 4b_j^2C_{11} & 4b_j^2C_{16}\\
-13b_jC_{16} & -13b_jC_{66} & -3b_j^2C_{16} & -3b_j^2C_{66} & -22b_jC_{16} & -22b_jC_{66} & 4b_j^2C_{16} & 4b_j^2C_{66}
\end{bmatrix}$$

$$[\mathbf{k}_{01}^j] = \frac{h}{60}\begin{bmatrix}
-30C_{16} & -30C_{66} & -6b_jC_{16} & -6b_jC_{66} & -30C_{16} & -30C_{66} & 6b_jC_{16} & 6b_jC_{66}\\
-30C_{12} & -30C_{26} & -6b_jC_{12} & -6b_jC_{26} & -30C_{12} & -30C_{26} & 6b_jC_{12} & 6b_jC_{26}\\
6b_jC_{16} & 6b_jC_{66} & 0 & 0 & -6b_jC_{16} & -6b_jC_{66} & b_j^2C_{16} & b_j^2C_{66}\\
6b_jC_{12} & 6b_jC_{26} & 0 & 0 & -6b_jC_{12} & -6b_jC_{26} & b_j^2C_{12} & b_j^2C_{26}\\
30C_{16} & 30C_{66} & 6b_jC_{16} & 6b_jC_{66} & 30C_{16} & 30C_{66} & -6b_jC_{16} & -6b_jC_{66}\\
30C_{12} & 30C_{26} & 6b_jC_{12} & 6b_jC_{26} & 30C_{12} & 30C_{26} & -6b_jC_{12} & -6b_jC_{26}\\
-6b_jC_{16} & -6b_jC_{66} & -b_j^2C_{16} & -b_j^2C_{66} & 6b_jC_{16} & 6b_jC_{66} & 0 & 0\\
-6b_jC_{12} & -6b_jC_{26} & -b_j^2C_{12} & -b_j^2C_{26} & 6b_jC_{12} & 6b_jC_{26} & 0 & 0
\end{bmatrix}$$

$$[\mathbf{k}_{00}^j] = \frac{h}{30b_j}\begin{bmatrix}
36C_{66} & 36C_{26} & 3b_jC_{66} & 3b_jC_{26} & -36C_{66} & -36C_{26} & 3b_jC_{66} & 3b_jC_{26}\\
36C_{26} & 36C_{22} & 3b_jC_{26} & 3b_jC_{22} & -36C_{26} & -36C_{22} & 3b_jC_{26} & 3b_jC_{22}\\
3b_jC_{66} & 3b_jC_{26} & 4b_j^2C_{66} & 4b_j^2C_{26} & -3b_jC_{66} & -3b_jC_{26} & -b_j^2C_{66} & -b_j^2C_{26}\\
3b_jC_{26} & 3b_jC_{22} & 4b_j^2C_{26} & 4b_j^2C_{22} & -3b_jC_{26} & -3b_jC_{22} & -b_j^2C_{26} & -b_j^2C_{22}\\
-36C_{26} & -36C_{26} & -3b_jC_{66} & -3b_jC_{26} & 36C_{66} & 36C_{26} & -3b_jC_{66} & -3b_jC_{26}\\
-36C_{26} & -36C_{22} & -3b_jC_{26} & -3b_jC_{22} & 36C_{26} & 36C_{22} & -3b_jC_{26} & -3b_jC_{22}\\
3b_jC_{66} & 3b_jC_{26} & -b_j^2C_{66} & -b_j^2C_{26} & -3b_jC_{66} & -3b_jC_{26} & 4b_j^2C_{66} & 4b_j^2C_{26}\\
3b_jC_{26} & 3b_jC_{22} & -b_j^2C_{26} & -b_j^2C_{22} & -3b_jC_{26} & -3b_jC_{22} & 4b_j^2C_{26} & 4b_j^2C_{22}
\end{bmatrix}$$

$$[\mathbf{m}^j] = \frac{\rho h b_j}{420}\begin{bmatrix}
156 & 0 & 22b_j & 0 & 54 & 0 & -13b_j & 0\\
0 & 156 & 0 & 22b_j & 0 & 54 & 0 & -13b_j\\
22b_j & 0 & 4b_j^2 & 0 & 13b_j & 0 & -3b_j^2 & 0\\
0 & 22b_j & 0 & 4b_j^2 & 0 & 13b_j & 0 & -3b_j^2\\
54 & 0 & 13b_j & 0 & 156 & 0 & -22b_j & 0\\
0 & 54 & 0 & 13b_j & 0 & 156 & 0 & -22b_j\\
-13b_j & 0 & -3b_j^2 & 0 & -22b_j & 0 & 4b_j^2 & 0\\
0 & -13b_j & 0 & -3b_j^2 & 0 & -22b_j & 0 & 4b_j^2
\end{bmatrix}.$$